ACS Medicinal Chemistry Letters

pubs.acs.org/acsmedchemlett

Letter

Unleashing the Potential of 1,3-Diketone Analogues as Selective LH2 Inhibitors

Juhoon Lee, Hou-fu Guo, Shike Wang, Yazdan Maghsoud, Erik Antonio Vázquez-Montelongo, Zhifeng Jing, Rae M. Sammons, Eun Jeong Cho, Pengyu Ren, G. Andrés Cisneros, Jonathan M. Kurie, and Kevin N. Dalby*

Cite This: *ACS Med. Chem. Lett.* 2023, 14, 1396−1403

Read Online

ACCESS | Metrics & More | Article Recommendations | Supporting Information

ABSTRACT: Lysyl hydroxylase 2 (LH2) catalyzes the formation of highly stable hydroxylysine aldehyde-derived collagen cross-links (HLCCs), thus promoting lung cancer metastasis through its capacity to modulate specific types of collagen cross-links within the tumor stroma. Using **1** and **2** from our previous high-throughput screening (HTS) as lead probes, we prepared a series of 1,3-diketone analogues, **1**−**18**, and identified **12** and **13** that inhibit LH2 with IC_{50}'s of approximately 300 and 500 nM, respectively. Compounds **12** and **13** demonstrate selectivity for LH2 over LH1 and LH3. Quantum mechanics/molecular mechanics (QM/MM) modeling indicates that the selectivity of **12** and **13** may stem from noncovalent interactions like hydrogen bonding between the morpholine/piperazine rings with the LH2-specific Arg661. Treatment of 344SQ WT cells with **13** resulted in a dose-dependent reduction in their migration potential, whereas the compound did not impede the migration of the same cell line with an LH2 knockout (LH2KO).

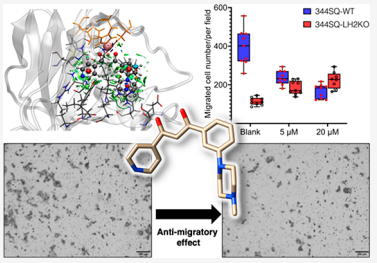

KEYWORDS: *Lysyl hydroxylase 2, LH2, α-Ketoglutarate, Hydroxylysine aldehyde-derived collagen cross-links, HLCC, Collagen, Inhibitor*

Lysyl hydroxylase 2 (LH2)-mediated telopeptidyl hydroxylysines form structurally rigid hydroxylysine aldehyde-derived collagen cross-links (HLCCs) resistant to cleavage by collagenases.[1] It is well-known that reduced lysine hydroxylation is a cause of genetic connective tissue disorders such as Bruck Syndrome,[2−6] while abnormally elevated HLCC formation is associated with fibrosis and cancer metastasis.[7−11]

Three lysyl hydroxylase isoforms (LH1−3) play essential roles in collagen modifications. Each isoform possesses two functionally distinct enzymatically active domains.[12] LH2 can hydroxylate Lys residues in the telopeptides, while all three LH isoforms hydroxylate lysine residues in the helical domain.[2] In fibrotic diseases of the lung[13] and liver,[14] HLCCs are the predominant types of cross-links attributable to excessive hydroxylation of the telopeptidyl Lys, owing to the overexpression of LH2 in fibroblasts.[8,15] A similar switch is associated with tumor stroma, where an increased level of LH2 leads to metastasis and is correlated with lower survival.[7,9] Heretofore, LH2 was thought to be localized in the ER, where it hydroxylates procollagen Lys residues before the triple helix formation.[16] However, it was recently found to modify collagen in the extracellular space as it is secreted by carcinoma cells.[17] It is shown to be expressed in cancer-associated fibroblasts and contributes to a switch toward a high-HLCC, low-LCC state in the tumor stroma.[18]

Minoxidil (Figure 1A), a widely recognized antifibrotic agent, was believed to reduce LH expression, thereby decreasing hydroxylysylpyridinoline cross-linking.[19] However,

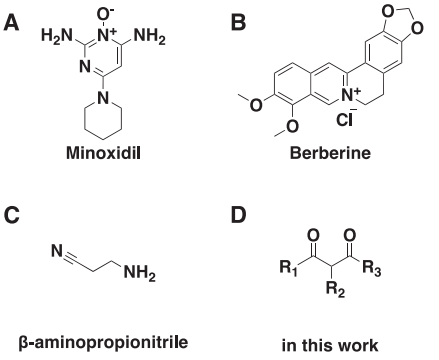

Figure 1. Compounds reported as LH2 inhibitors.

Pfeffer et al. found that minoxidil does not significantly impact LH activity during postnatal mouse lung development.[20] Berberine (Figure 1B) inhibits LH2 expression in TNBC cells, reducing the proliferation, motility, and glycolysis. This is achieved by suppressing interleukin-6 (IL-6) secretion, indirectly regulating LH2 activity.[21] *β*-Aminopropionitrile

Received: July 12, 2023
Accepted: September 13, 2023
Published: September 22, 2023

https://doi.org/10.1021/acsmedchemlett.3c00305
ACS Med. Chem. Lett. 2023, 14, 1396−1403

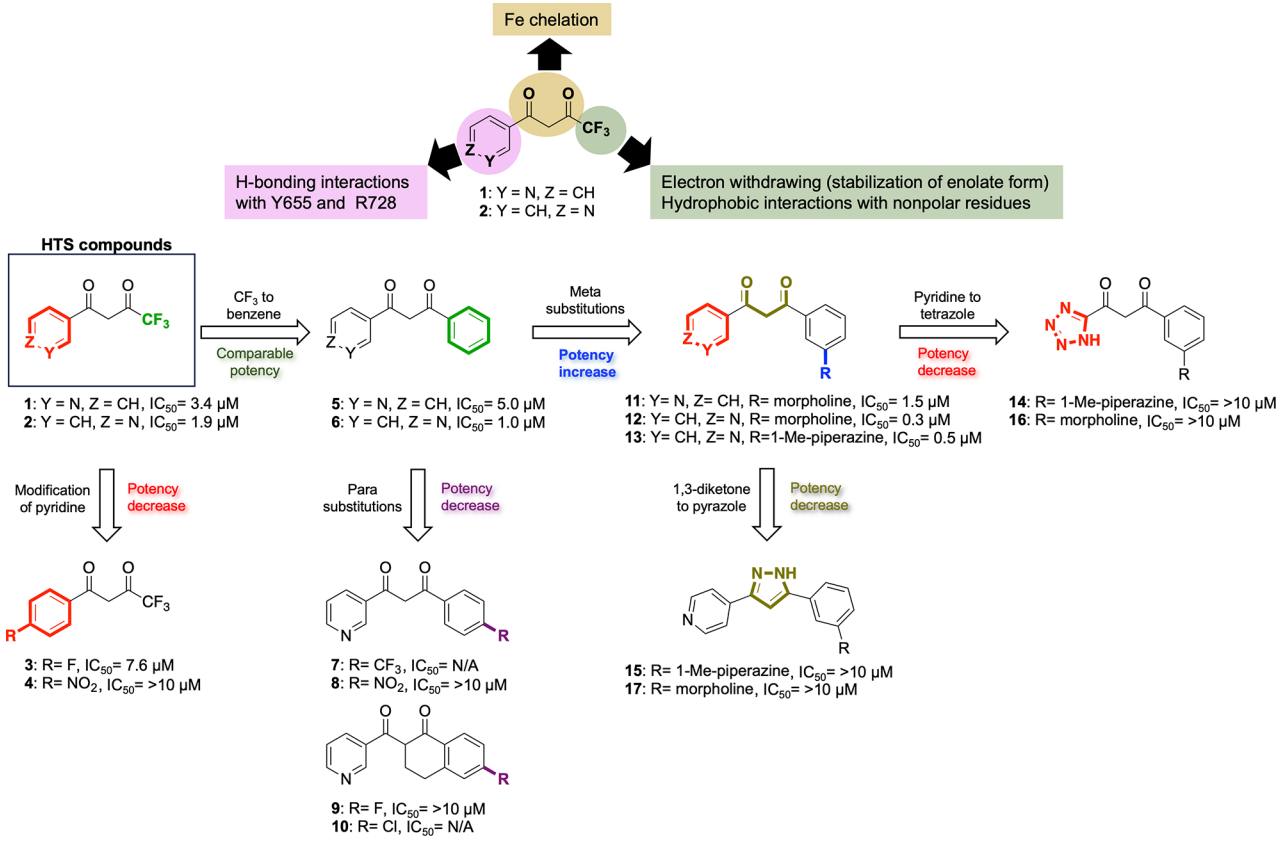

Figure 2. Rational design flowcharts of LH2 inhibitors.

(Figure 1C) has been observed to induce downregulation of LH2 expression and impede the formation of a stable matrix, likely by direct inhibition of LOX family members.[22]

Our previous high-throughput screening utilizing luminescence-based lysyl hydroxylase activity assay identified two 1,3-diketone analogues (Figure 1D and compounds **1** and **2** in Figure 2) with IC_{50} values of 3.4 and 1.9 μM, respectively.[31] The same assay conducted in the presence of an excess of Fe^{2+} demonstrated that the activity of **1** arises from its direct interaction with the enzyme rather than any interference with the assay components (Figure S48). While 1,3-diketone analogues are widely distributed in natural products and exhibit various pharmacological activities, including antibacterial, antioxidant, antiviral, insecticidal, and antifungal properties,[23−27] their inhibition activity toward LH2 has not been reported. Notably, owing to their inherent tautomerism, these compounds are uniquely poised to engage in metal chelation and hydrogen bonding, endowing them with considerable potential as a molecular scaffold for intermediates in various organic reactions, metal−organic hybrid materials, and novel drug design.[28,29] Indeed, our molecular docking studies confirmed the chelation of Fe(II) by the dicarbonyl moiety and hydrogen bonding of the pyridine nitrogen with LH2 active-site residues (Y655 and R728, human PLOD2), as illustrated in Figure 3A,B, providing a foundation for compounds **1** and **2** as leading probes for further optimization.

Here we report a structure-based rational design strategy of 1,3-diketone analogues (compounds **1**−**18**) as LH2 inhibitors along with their inhibitory activity and computation investigation. Although compounds **1**−**8** were previously known, their biological activity against LH2 has not been studied. Compounds **9**−**18** were newly designed specifically for this

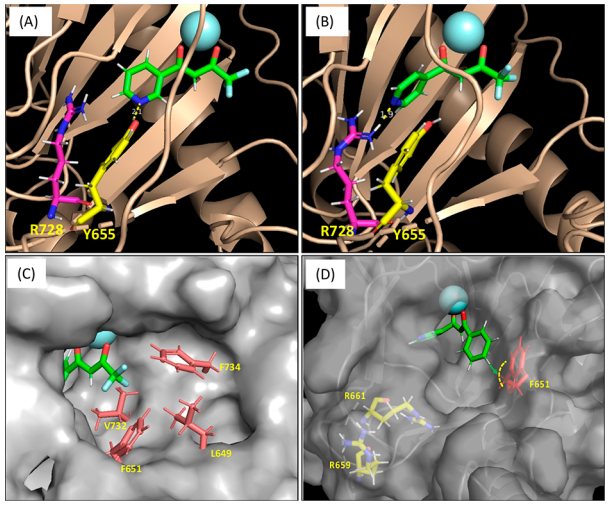

Figure 3. Binding interactions between HTS hit compounds **1** (A and C), **2** (B), and **5** (C) and the LH2 active site predicted by molecular docking studies and observed in MD and QM/MM simulations. (A) Calculated distance between the phenol hydrogen (Y655) and the pyridine nitrogen of **1** is 2.1 Å. (B) Calculated distance between the guanidine hydrogen (R728) and the pyridine nitrogen of **2** is 1.9 Å. (C) The entry of the active site of LH2 associated with **1** shows the hydrophobic environment in proximity to trifluoromethyl ($-CF_3$) group of 1. (D) Docked model of **5** presenting the surface environment of the benzene ring of the compound.

study. The 1,3-diketone analogues were synthesized as depicted in Scheme 1. Compounds **3** and **4** were prepared via modified Claisen condensation.[29] Compounds **5**−**10** were synthesized from acyl chlorides with enolated ketones by soft

https://doi.org/10.1021/acsmedchemlett.3c00305
ACS Med. Chem. Lett. 2023, 14, 1396−1403

Scheme 1. Synthesis of Inhibitors 3−18

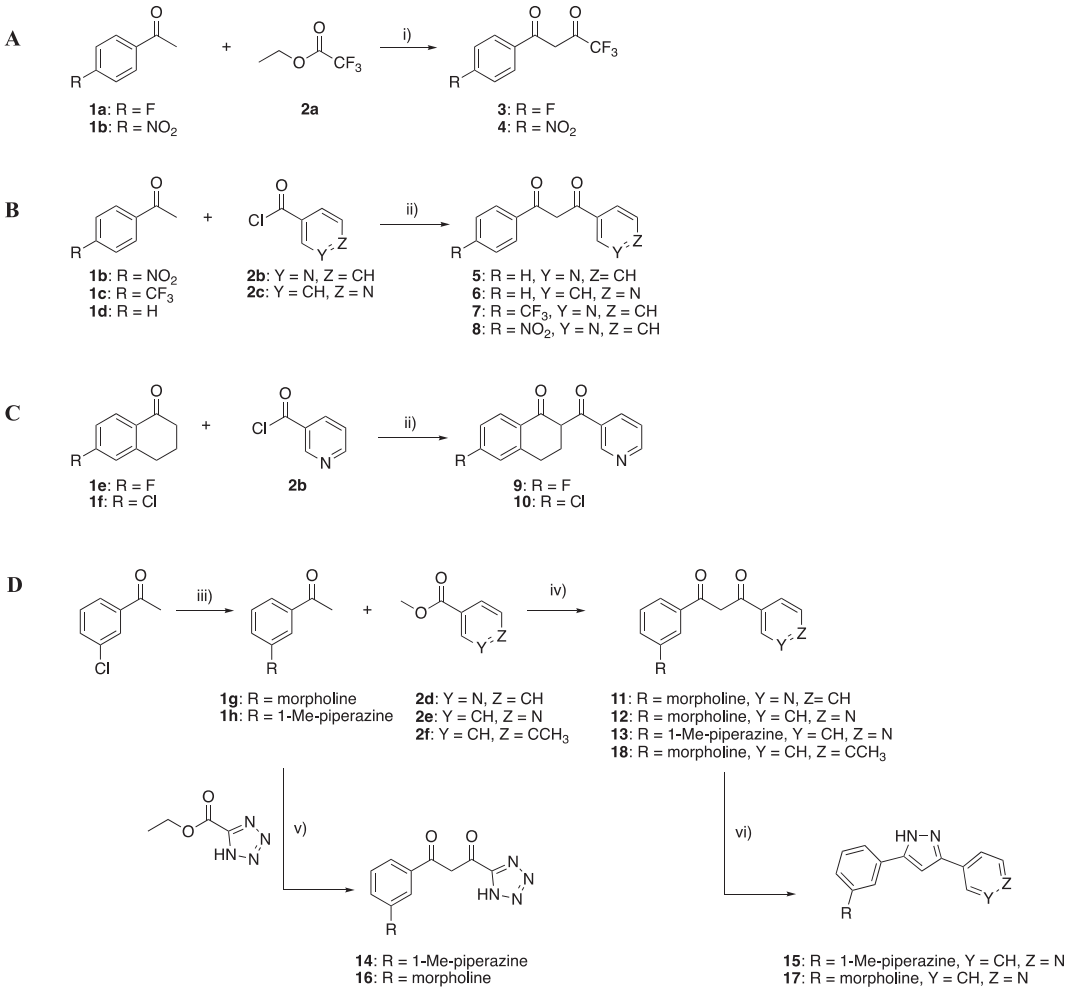

[a]Reagents and reaction conditions: (i) NaH, THF, 0 °C to RT, 12 h; (ii) $MgBr_2$·OEt, DIPEA, DCM, RT, 12 h; (iii) 3-chloroacetopheone, morpholine or 1-methyl-piperazine, Pd_2 (dba)$_3$, DavePhos, K_3PO_4, DME, Ar, 100 °C, 12 h; (iv) LiN(SiMe$_3$)$_2$, Ar, THF, −40 °C, 6 h; (v) (a) 2-methoxypropene, p-TSA, THF, RT, 1 h. (b) LiN(SiMe$_3$)$_2$, Ar, THF, −40 °C, 6 h, (c) HCl; vi) NH_2NH_2·H_2O, ethanol, RT, 12 h.

enolization[30] in the presence of magnesium bromide diethyl etherate and Hünig's base. **11**−**13**, and **18** were synthesized from acylation of meta-substituted acetophenones **1g**−**1h** with esters **2d**−**2f** in the presence of lithium bis(trimethylsilyl) amide. The meta-substituted acetophenones also underwent an acylation reaction with 2-methoxypropyl-protected ethyl tetrazole-5-carboxylate to afford tetrazole-substituted variants **14** and **16**. Pyrazole-substituted derivatives **15** and **17** were prepared by reacting **12** or **13** with hydrazine monohydrate in ethanol.

Previously, we conducted an exhaustive computational investigation on forty-four molecules,[32] which included most of the compounds discussed in this paper. Based on polarizable molecular dynamics (MD) simulation and coupled quantum mechanics/molecular mechanics (QM/MM) optimizations, we found that the enolate forms of **1** and **2** have considerably strong interactions with the active site (−169.4 and −139.7 kcal mol^{-1}, respectively) as well as several NCIs (noncovalent interactions) with the residues of the active site including Y655 and R728.

First, compounds **3** and **4** featuring para-substituted benzene rings in the R_1 position were prepared to investigate the involvement of pyridine in the interaction with inner residues Y655 and R728. These compounds displayed diminished inhibitory activity relative to **1** and **2** and weaker calculated polarizable QM/MM interaction with LH2 (−50.4 and −38.7 kcal mol^{-1}, respectively),[32] underscoring the necessity of pyridine in mediating the interaction with the LH2 active site.

We then implemented a modification to the R_3 position. We hypothesized that the trifluoromethyl (−CF_3) group plays a role not only in withdrawing electron density, which stabilizes the formation of an enolate but also interacts with nonpolar residues situated at the entrance of the LH2 active site via hydrophobic interactions, as shown in Figure 3C. Thus, we opted to substitute the trifluoromethyl group with a benzene ring, which is considered to possess similar characteristics, along with better accessibility for functionalization. Notably, **5** (IC_{50} = 5.0 μM) and **6** (IC_{50} = 1.0 μM) retained inhibitory activity relative to the original hits from HTS. Compared with compounds **1** and **2**, compounds **5**[32] and **6** (Table S2) show considerably stronger interactions with the LH2 (−185.2 and −200.1 kcal mol^{-1}, respectively).

We further functionalized compound **5** by introducing additional groups at the para position of the benzene ring (**7** and **8**) and at the 6-position of the tetralin group, which is linked to the R_2 position (**9** and **10**). However, including

https://doi.org/10.1021/acsmedchemlett.3c00305
ACS Med. Chem. Lett. 2023, 14, 1396−1403

functional groups at the para position of the benzene led to a decrease in the potency of the compounds (**7**; IC_{50} = N/A, **8**; IC_{50} = > 10 μM, **9**; IC_{50} = > 10 μM, **10**; IC_{50} = N/A). This implies that the para position of the benzene ring may offer restricted space for functional groups to occupy, which is further corroborated by the molecular docking analysis and MD simulation of compound **5** onto the LH2 homology model, as depicted in Figure 3D. The calculated QM/MM interaction energies ($IE_{QM/MM}$) for compounds **7**−**10** were −114.2, −190.5, −212.6, and −212.9 kcal mol^{-1}, respectively.[32] This suggests that the presence of $-CF_3$ in the para position of the benzene ring in compound **7** led to a significant decrease in the interaction energies. At the same time, it was slightly increased for the other three compounds compared to compound **5**. Interestingly, the number of residues having noncovalent interactions with these four compounds showed a slight decrease compared to compound **5**, especially in the case of compounds **7** and **9**.[32] This suggested that our modifications at the para position of the benzene ring do not improve interaction between the inhibitor and the residues at the binding pocket. Given the LH2−inhibitor interaction energies, noncovalent interactions, and distinct hindrance by F651 on the para-modification, we investigated whether a meta-substitution could enhance binding to LH2.

The docked model of **5** revealed possible additional recognition sites, R661 and R659, proximal to the meta position of the benzene of **5** (Figure 3D). This was later supported by MD simulation of the ligand-bound system of this compound.[32] These two basic amino acid residues adjacent to the LH2 active site are specific to this member of the LH family. (The corresponding residues in LH1 and LH3 are Glu and Pro, respectively.) These residues are thought to play a role in the electrostatic interactions with acidic aspartate and glutamate residues positioned adjacent to the Lys residues on fibrillar collagens.[12] We postulated that LH2's unique telopeptidyl lysyl hydroxylase activity and selectivity are determined partly by electrostatic interactions between the basic domain of LH2 and the acidic domain of collagen telopeptides. To achieve favorable interactions with the basic residues, morpholine (**11** and **12**) and 1-methyl piperazine (**13**) rings, which possess the intrinsic capability to participate in hydrogen bonding[33,34] were incorporated at the meta-position of the benzene of compounds **5** and **6**. Introducing the meta-substituted morpholine and methyl piperazine rings boosts the potencies (**11**; IC_{50} = 1.5 μM, **12**; IC_{50} = 0.3 μM, and **13**; IC_{50} = 0.5 μM) compared with the parent inhibitors **5** and **6**. Notably, the weaker potency of **11** compared to that of **12** indicates that the pyridine nitrogen atom in the 4-position is optimal for interacting with inner residues in the active site.

The results of $IE_{QM/MM}$ between compounds **12** and **13** with LH2 are −259.9 and −216.3 kcal mol^{-1}, respectively (see Table S2). The low values of $IE_{QM/MM}$ suggest a strong interaction between these two analogues and the enzyme. Table S2 also shows that the calculated interactions due to the QM region in compounds **12** and **13** are similar, −197.6 and −197.4 kcal mol^{-1}, respectively, but the interactions due to the MM region in compound **12** are about three times greater than those in compound **13** (−62.3 and −18.9 kcal mol^{-1}, respectively). In the case of **6**, the interaction is weaker than the other two but the MM region stability is enhanced compared with the other two ligands.

A closer look into the NCI plots shows that compound **12** has two hydrogen bonds with R728 and R661 (Figure 4A-middle), and compound **13** has weak interactions with R661 (Figure 4A-right). In comparison, compound **6** only has two hydrogen bonds with two water molecules in the active site (Figure 4A-left). The interactions of **12** and **13**, particularly with the R661 residue, suggest that their potencies might derive from the engagement of morpholine and methyl piperazine rings with LH2-specific R661.

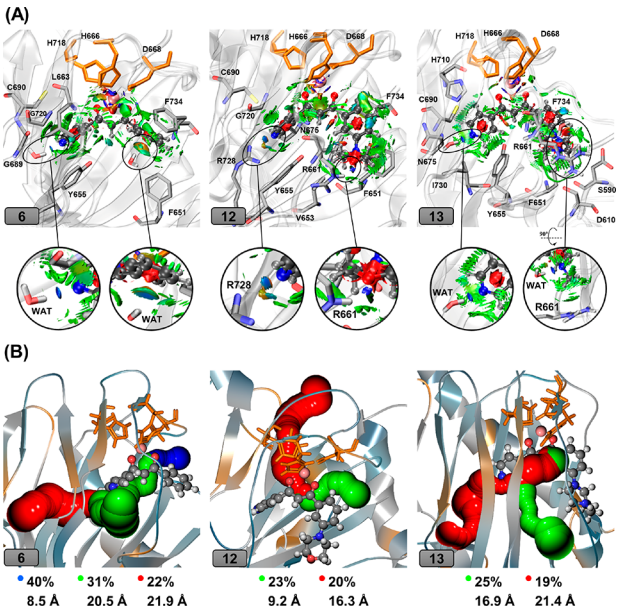

Figure 4. (A) The plot of the noncovalent interactions between compounds **6**, **12**, and **13** and the surrounding amino acid residues. The inhibitors are given in ball-and-sticks, and Fe(II) is shown in pink sphere. Residues forming noncovalent interactions with the inhibitor are shown in sticks. Red surfaces are related to repulsive interactions, while green surfaces denote weak interactions like van der Waals, and blue ones show strong attractive interactions such as hydrogen bonds. (B) O_2-transporting tunnels with largest calculated percentages along the trajectory observed in compounds **6**, **12**, and **13**. Calculated tunnels are colored in blue, green, and red, respectively, based on the tunnel's length (Å) (blue: shortest, red: longest).

Our previous study suggested that three major tunnels exist in the apo-LH2, which can transport molecular oxygen to the active site, with tunnel availability probabilities of 63%, 51%, and 32% for blue, green, and red tunnels, respectively.[32] Our results also showed that compounds **7** and **8** and some other studied molecules in that study considerably decreased the availability of these tunnels and elongated the tunnels' lengths. As seen in Figure 4B, the tunneling results for compounds **6**, **12**, and **13** showed the same trend in which the availability/length of the tunnels decreased/increased. Interestingly, in the case of compounds **12** and **13**, only two major putative tunnels are available for oxygen transportation.

A final set of modifications were performed, based on **12** and **13**, by replacing the pyridine moiety with tetrazole (**16**; IC_{50} = > 10 μM, **14**; IC_{50} = > 10 μM) and the 1,3-diketone with pyrazole (**17**; IC_{50} = > 10 μM, **15**; IC_{50} = > 10 μM). The results indicated that pyridine and 1,3-diketone scaffolds are essential for the activity of the studied compounds. In addition, **18** with the toluene group on the R_1 position shows no activity, supporting the importance of pyridine.

https://doi.org/10.1021/acsmedchemlett.3c00305
ACS Med. Chem. Lett. 2023, 14, 1396−1403

In light of the initial investigation of the structure−activity relationship (SAR) using a luminescence-based LH activity assay (Table 1) and further supported by computational studies, the HTS hit compounds (**1** and **2**) and the four most potent compounds (**6**, **11**, **12**, and **13**) were further evaluated using the same activity assay against all three LH isoforms for selectivity profiling (Table 2). Compounds **12** and **13** exhibited the most promising LH2 selectivity among the six inhibitors tested. Specifically, the inhibition potency of compound **12** against LH2 was approximately 8-fold and 9-fold stronger than those against LH1 and LH3, respectively. In the case of **13**, the LH2 selectivity over LH3 was observed as 9-fold, while it displayed a relatively lower selectivity (3-fold) over LH1. These results indicate that the engagement of the morpholine and methyl piperazine rings with the LH2-specific residue R661 is responsible for the selective binding to LH2.

Table 1. SAR of 1,3-Diketone Analogues

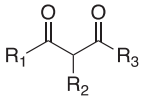

Cpds	R_1	R_2	R_3	IC_{50} (μM)[a]
1	3-Py[b]	H	CF_3	3.4 ± 1.1
2	4-Py	H		1.9 ± 0.6
3	4-F-Ph[b]	H		7.6 ± 2.9
4	4-NO_2-Ph	H		>10
5	3-Py	H	Ph	5.0 ± 1.9
6	4-Py	H		1.0 ± 0.9
7	3-Py	H	4-CF_3-Ph	N/A
8	3-Py	H	4-NO_2-Ph	>10
9	3-Py			>10
10	3-Py			N/A
11	3-Py	H		1.5 ± 0.5
12	4-Py	H		0.3 ± 0.1
13	4-Py	H		0.5 ± 0.1
14	Tetrazole	H		>10
16	Tetrazole	H		>10
18	4-Me-Ph	H		N/A
15	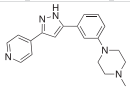			>10
17	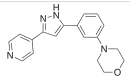			>10

[a]IC_{50} values were measured using a luminescence-based LH activity assay against LH2. See Supporting Information for a detailed description of the assay conditions. [b]Py = pyridyl, Ph = phenyl

Table 2. Selectivity of Inhibitors toward All Three LH Isoforms

	IC_{50} (μM)[a]		
Cpds	LH2	LH1	LH3
1	3.4 ± 1.1	4.3 ± 1.3	5.2 ± 4.0
2	1.9 ± 0.6	4.8 ± 0.9	4.8 ± 0.8
6	1.0 ± 0.9	6.4 ± 8.0	5.2 ± 6.0
11	1.5 ± 0.5	1.7 ± 0.8	4.8 ± 1.9
12	0.3 ± 0.1	2.3 ± 0.9	2.7 ± 2.9
13	0.5 ± 0.1	1.6 ± 0.6	4.7 ± 8.8

[a]IC_{50} values were measured using a luminescence-based LH activity assay. See Supporting Information for a detailed description of the assay conditions.

Compound **6** demonstrated modest selectivity toward LH2, with 6-fold and 5-fold more potency than LH1 and LH3, respectively, while compounds **1**, **2**, and **11** showed less than 3-fold or no selectivity. The moderate selectivity of compound **6** can be attributed to the hydrophobic interactions between the benzene ring of **6** and hydrophobic residues (F651 and F734) at the entry of the active site, which aids in the stable binding to LH2, as shown in Figure 4A.

To further assess the selectivity of compounds **6**, **12**, and **13**, we subjected them to screening against other Fe(II)/2OG-dependent enzymes. These enzymes included FTO (fat mass and obesity-associated protein, which preferentially demethylates N^6-methyladenosine in RNA[35]), JMJD2A (the histone demethylase Jumonji domain-containing protein 2A[36]), EGLN1 (Egl-9 family hypoxia-inducible factor 1, also called prolyl hydroxylase domain-containing protein 2 or PHD2[37]), and mimivirus L230, which hydroxylates lysine and glycosylates hydroxylysine residues on collagen.[38] The percent inhibition of each of these enzymes at a dose of 11 μM compound (**6**, **12**, or **13**) is shown in Figure 5. The results indicate that all three compounds display a more pronounced inhibitory effect toward LH2 than other enzymes. Compound **6** shows lower selectivity for LH2 than the other compounds as it inhibits JMJD2A similarly to LH2.

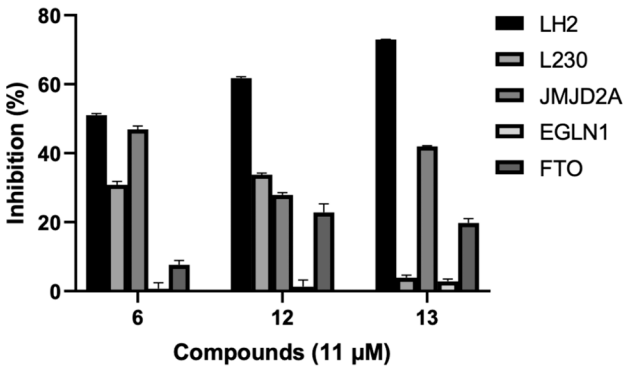

Figure 5. Selectivity profile of compounds against other Fe(II)/2OG-dependent enzymes. Compounds **6**, **12**, and **13** were tested at 11 μM for inhibition of LH2 and other Fe(II)/2OG-dependent enzymes L230, JMJD2A, EGLN1, and FTO. Inhibition (%) is the percent decrease in the luminescence signal relative to DMSO controls in the luminescence-based selectivity assay. All samples were performed in duplicate, and error bars indicate standard error.

High expression of LH2 has been shown to drive cell migration in multiple cancer types.[12,39,40] To determine if the most potent compounds identified in our study have selective activity against LH2 in cells, we evaluated the inhibitory effect of representative compound **13** on metastatic murine NSCLC (nonsmall cell lung cancer) cell line 344SQ that harbor mutations in Kras and p53.[41] We used the parental 344SQ, Crispr-Cas9 edited LH2 KO 344SQ cell lines for the proliferation and migration assays.

https://doi.org/10.1021/acsmedchemlett.3c00305
ACS Med. Chem. Lett. 2023, 14, 1396−1403

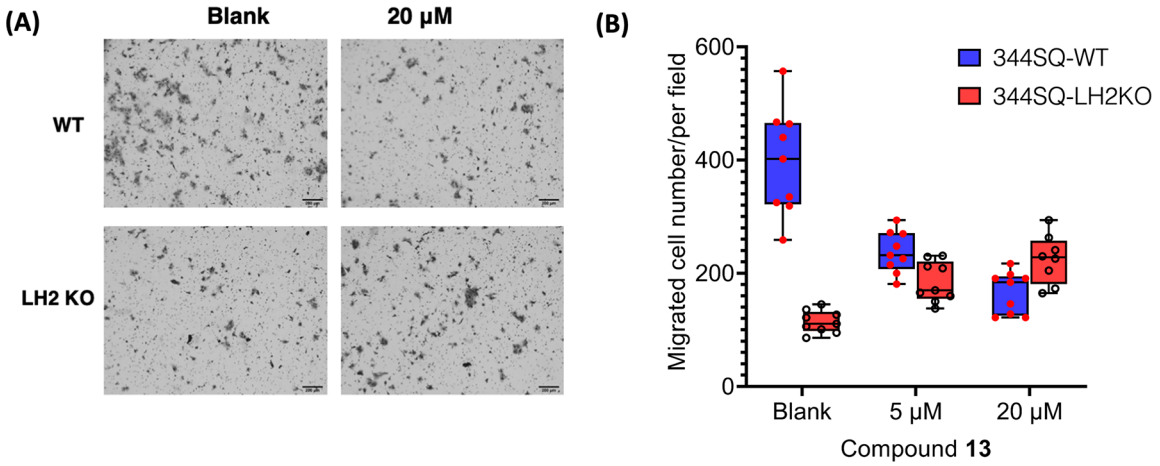

Figure 6. Cell migration assay. Compound **13** suppresses cell migration of 344SQ lung adenocarcinoma cells (LH2b is highly expressed). A) Migrated 344SQ cells (WT and LH2 KO) in Boyden chambers were imaged after treatment with vehicle control (blank) and 20 μM of **13**. B) Migrated 344SQ cells were counted after treatment with vehicle control (blank), 5 μM, and 20 μM of **13**. Triplicates were performed for each condition, and the migration assay was repeated twice independently. When compared to 344SQ-WT cells treated with vehicle control (blank), 5 μM, and 20 μM of **13**, a two-sided Student's *t*-test analysis gave values of p = 0.000006, 0.001, and 0.07 for the corresponding concentrations of **13** in 344SQ LH2KO cells, respectively.

Figure 6 shows that compound **13** demonstrated a dose-dependent inhibition on the parental 344SQ cells. In contrast, it was observed that compound **13** did not exert any obvious impact on the proliferation of parental 344SQ cells at the concentrations that were tested (Figure S47). Importantly, the compound did not hamper the migration of LH2KO cells, as depicted in Figures 6A and B, strongly suggesting its discerning activity for LH2 in both in vitro and cellular settings.

Notably, LH2KO cells were employed as a reference control to investigate whether the inhibitory effect of compound **13** is solely due to its action on LH2 or whether it interferes with other targets. If compound **13** targets additional molecules that promote cell migration, then it would still exhibit an inhibitory effect. Although there is no statistically significant difference between the migrations of WT and LH2KO cells treated with 20 μM compound **13** (p-value = 0.07 based on nine readings from a two-sided Student's *t* test analysis), the observation that compound **13** induces a slight increase in the migration of LH2KO cells is intriguing. One plausible explanation for this observation is that compound **13** shows preferential binding to LH2 in the presence of LH2. In contrast, the compound interacts with alternative targets in its absence, resulting in the observed effect. Further experiments are underway to explore the potential alternative targets of compound **13** and to elucidate the mechanisms underlying its effect on cell migration in LH2KO cells.

In conclusion, the current study delineates the synthesis, design, and evaluation of a series of 18 1,3-diketone analogues (compounds **1**–**18**) with respect to their potential to inhibit the LH2 enzymatic activity through luciferase-based biochemical and cell migration assays. The pyridine moiety at R_1 was found to be a prerequisite for efficient hydrogen-bonding interactions with LH2's active site residues. R_3 was tailored to accommodate a benzene ring, replacing the trifluoromethyl group in the HTS compounds. Meta-substitution of the benzene ring conveys an advantageous effect on the LH2 inhibitory activity, whereas para-modification attenuates potency due to hindrance by F651. Notably, compounds **12** and **13**, featuring morpholine and 1-methyl piperazine, respectively, on the meta position of the benzene moiety, exhibit improved potencies and selectivity for LH2 compared with the other isoforms and Fe(II)/2OG-dependent enzymes.

Further investigations by MD and QM/MM calculations suggest that **12** and **13** can firmly interact with the enzyme, corroborating their inhibitory activities and selectivity. Migration assays in the 344SQ lung adenocarcinoma cell line reveal that compound **13** demonstrates a dose-dependent antimigratory effect. While we acknowledge that there is still much to be done in the field of LH2 inhibition for the treatment of cancer metastasis, the findings presented in this study may represent a significant step forward in developing potential LH2 inhibitors, particularly given the limited availability of effective LH2 antagonists.

■ ASSOCIATED CONTENT

Supporting Information

The Supporting Information is available free of charge at https://pubs.acs.org/doi/10.1021/acsmedchemlett.3c00305.

Supplementary figures and tables, as well as synthetic procedures, NMR, ESI-MS characterization, material and methods for biological assays, computational methods, and analysis (PDF)

Additional ESI for the AMOEBA parameters for all the studied compounds (ZIP)

■ AUTHOR INFORMATION

Corresponding Author

Kevin N. Dalby − *Division of Chemical Biology and Medicinal Chemistry, College of Pharmacy, University of Texas at Austin, Austin, Texas 78712, United States; Targeted Therapeutic Drug Discovery and Development Program, College of Pharmacy, University of Texas, Austin, Texas 78712, United States;* orcid.org/0000-0001-9272-5129; Email: dalby@austin.utexas.edu

Authors

Juhoon Lee − *Division of Chemical Biology and Medicinal Chemistry, College of Pharmacy, University of Texas at Austin, Austin, Texas 78712, United States; Targeted Therapeutic Drug Discovery and Development Program,*

https://doi.org/10.1021/acsmedchemlett.3c00305
ACS Med. Chem. Lett. 2023, 14, 1396−1403

College of Pharmacy, University of Texas, Austin, Texas 78712, United States; orcid.org/0000-0001-7178-4226

Hou-fu Guo − *Department of Molecular and Cellular Biochemistry, University of Kentucky College of Medicine, Lexington, Kentucky 40536, United States*

Shike Wang − *Department of Thoracic/Head and Neck Medical Oncology, The University of Texas MD Anderson Cancer Center, Houston, Texas 77030, United States*

Yazdan Maghsoud − *Department of Chemistry and Biochemistry, The University of Texas at Dallas, Richardson, Texas 75080, United States;* orcid.org/0000-0002-4051-0844

Erik Antonio Vázquez-Montelongo − *Department of Physical Medicine and Rehabilitation, The University of Texas Southwestern Medical Center, Dallas, Texas 75390, United States;* orcid.org/0000-0001-5253-7887

Zhifeng Jing − *Department of Biomedical Engineering, The University of Texas at Austin, Austin, Texas 78712, United States;* orcid.org/0000-0001-7013-036X

Rae M. Sammons − *Division of Chemical Biology and Medicinal Chemistry, College of Pharmacy, University of Texas at Austin, Austin, Texas 78712, United States; Targeted Therapeutic Drug Discovery and Development Program, College of Pharmacy, University of Texas, Austin, Texas 78712, United States*

Eun Jeong Cho − *Division of Chemical Biology and Medicinal Chemistry, College of Pharmacy, University of Texas at Austin, Austin, Texas 78712, United States; Targeted Therapeutic Drug Discovery and Development Program, College of Pharmacy, University of Texas, Austin, Texas 78712, United States*

Pengyu Ren − *Department of Biomedical Engineering, The University of Texas at Austin, Austin, Texas 78712, United States;* orcid.org/0000-0002-5613-1910

G. Andrés Cisneros − *Department of Chemistry and Biochemistry, The University of Texas at Dallas, Richardson, Texas 75080, United States; Department of Physics, The University of Texas at Dallas, Richardson, Texas 75080, United States;* orcid.org/0000-0001-6629-3430

Jonathan M. Kurie − *Department of Thoracic/Head and Neck Medical Oncology, The University of Texas MD Anderson Cancer Center, Houston, Texas 77030, United States*

Complete contact information is available at: https://pubs.acs.org/10.1021/acsmedchemlett.3c00305

Author Contributions

The manuscript was written through contributions of all authors. All authors have approved the final version of the manuscript.

Notes

The authors declare no competing financial interest.

■ ACKNOWLEDGMENTS

This work was supported by NIH CA070907, CPRIT RP210088, WELCH F-1390 (K.N.D); NIH R00CA225633, University of Kentucky Center for Cancer and Metabolism, funded through the NIH/NIGMS COBRE program under grant number P20 GM121327 (H.G.); NIH R01GM106137, R01GM114237 (P.R); NIH CA251067 (J.M.K); R01GM108583, computing from XSEDE through allocation TG-CHE160044, UNT CASCaM (partially funded by the NSF Grant Nos. CHE1531468 and OAC-2117247) and UT-Dallas' Cyberinfrastructure and Research Services (G.A.C.).

■ ABBREVIATIONS

THF, tetrahydrofuran; DIPEA, *N,N*-diisopropylethylamine; DCM, dichloromethane; DME, dimethoxyethane; p-TSA, p-toluenesulfonic acid; QM/MM, quantum mechanics/molecular mechanics; NCI, noncovalent interactions

■ REFERENCES

(1) Yamauchi, M.; Sricholpech, M. Lysine post-translational modifications of collagen. *Essays Biochem* **2012**, *52*, 113−33.

(2) Scietti, L.; Campioni, M.; Forneris, F. SiMPLOD, a Structure-Integrated Database of Collagen Lysyl Hydroxylase (LH/PLOD) Enzyme Variants. *J. Bone Miner Res.* **2019**, *34* (7), 1376−1382.

(3) Hyland, J.; Ala-Kokko, L.; Royce, P.; Steinmann, B.; Kivirikko, K. I.; Myllyla, R. A homozygous stop codon in the lysyl hydroxylase gene in two siblings with Ehlers-Danlos syndrome type VI. *Nat. Genet.* **1992**, *2* (3), 228−31.

(4) Ha-Vinh, R.; Alanay, Y.; Bank, R. A.; Campos-Xavier, A. B.; Zankl, A.; Superti-Furga, A.; Bonafe, L. Phenotypic and molecular characterization of Bruck syndrome (osteogenesis imperfecta with contractures of the large joints) caused by a recessive mutation in PLOD2. *Am. J. Med. Genet A* **2004**, *131A* (2), 115−120.

(5) Vahidnezhad, H.; Youssefian, L.; Saeidian, A. H.; Touati, A.; Pajouhanfar, S.; Baghdadi, T.; Shadmehri, A. A.; Giunta, C.; Kraenzlin, M.; Syx, D.; Malfait, F.; Has, C.; Lwin, S. M.; Karamzadeh, R.; Liu, L.; Guy, A.; Hamid, M.; Kariminejad, A.; Zeinali, S.; McGrath, J. A.; Uitto, J. Mutations in PLOD3, encoding lysyl hydroxylase 3, cause a complex connective tissue disorder including recessive dystrophic epidermolysis bullosa-like blistering phenotype with abnormal anchoring fibrils and type VII collagen deficiency. *Matrix Biol.* **2019**, *81*, 91−106.

(6) Salo, A. M.; Cox, H.; Farndon, P.; Moss, C.; Grindulis, H.; Risteli, M.; Robins, S. P.; Myllyla, R. A connective tissue disorder caused by mutations of the lysyl hydroxylase 3 gene. *Am. J. Hum. Genet.* **2008**, *83* (4), 495−503.

(7) Chen, Y.; Terajima, M.; Yang, Y.; Sun, L.; Ahn, Y. H.; Pankova, D.; Puperi, D. S.; Watanabe, T.; Kim, M. P.; Blackmon, S. H.; Rodriguez, J.; Liu, H.; Behrens, C.; Wistuba, I. I.; Minelli, R.; Scott, K. L.; Sanchez-Adams, J.; Guilak, F.; Pati, D.; Thilaganathan, N.; Burns, A. R.; Creighton, C. J.; Martinez, E. D.; Zal, T.; Grande-Allen, K. J.; Yamauchi, M.; Kurie, J. M. Lysyl hydroxylase 2 induces a collagen cross-link switch in tumor stroma. *J. Clin Invest* **2015**, *125* (3), 1147−62.

(8) van der Slot, A. J.; Zuurmond, A. M.; van den Bogaerdt, A. J.; Ulrich, M. M.; Middelkoop, E.; Boers, W.; Karel Ronday, H.; DeGroot, J.; Huizinga, T. W.; Bank, R. A. Increased formation of pyridinoline cross-links due to higher telopeptide lysyl hydroxylase levels is a general fibrotic phenomenon. *Matrix Biol.* **2004**, *23* (4), 251−7.

(9) Eisinger-Mathason, T. S.; Zhang, M.; Qiu, Q.; Skuli, N.; Nakazawa, M. S.; Karakasheva, T.; Mucaj, V.; Shay, J. E.; Stangenberg, L.; Sadri, N.; Pure, E.; Yoon, S. S.; Kirsch, D. G.; Simon, M. C. Hypoxia-dependent modification of collagen networks promotes sarcoma metastasis. *Cancer Discov* **2013**, *3* (10), 1190−205.

(10) Yamauchi, M.; Barker, T. H.; Gibbons, D. L.; Kurie, J. M. The fibrotic tumor stroma. *J. Clin Invest* **2018**, *128* (1), 16−25.

(11) Piersma, B.; Bank, R. A. Collagen cross-linking mediated by lysyl hydroxylase 2: an enzymatic battlefield to combat fibrosis. Essays. *Biochem* **2019**, *63* (3), 377−387.

(12) Guo, H. F.; Bota-Rabassedas, N.; Terajima, M.; Leticia Rodriguez, B.; Gibbons, D. L.; Chen, Y.; Banerjee, P.; Tsai, C. L.; Tan, X.; Liu, X.; Yu, J.; Tokmina-Roszyk, M.; Stawikowska, R.; Fields, G. B.; Miller, M. D.; Wang, X.; Lee, J.; Dalby, K. N.; Creighton, C. J.; Phillips, G. N., Jr; Tainer, J. A.; Yamauchi, M.; Kurie, J. M. A collagen glucosyltransferase drives lung adenocarcinoma progression in mice. *Commun. Biol.* **2021**, *4* (1), 482.

(13) Last, J. A.; King, T. E., Jr; Nerlich, A. G.; Reiser, K. M. Collagen cross-linking in adult patients with acute and chronic fibrotic lung disease. Molecular markers for fibrotic collagen. *Am. Rev. Respir. Dis.* **1990**, *141* (2), 307−13.
(14) Perepelyuk, M.; Terajima, M.; Wang, A. Y.; Georges, P. C.; Janmey, P. A.; Yamauchi, M.; Wells, R. G. Hepatic stellate cells and portal fibroblasts are the major cellular sources of collagens and lysyl oxidases in normal liver and early after injury. *Am. J. Physiol Gastrointest Liver Physiol* **2013**, *304* (6), G605−14.
(15) van der Slot, A. J.; Zuurmond, A. M.; Bardoel, A. F.; Wijmenga, C.; Pruijs, H. E.; Sillence, D. O.; Brinckmann, J.; Abraham, D. J.; Black, C. M.; Verzijl, N.; DeGroot, J.; Hanemaaijer, R.; TeKoppele, J. M.; Huizinga, T. W.; Bank, R. A. Identification of PLOD2 as telopeptide lysyl hydroxylase, an important enzyme in fibrosis. *J. Biol. Chem.* **2003**, *278* (42), 40967−72.
(16) Myllyharju, J.; Kivirikko, K. I. Collagens, modifying enzymes and their mutations in humans, flies and worms. *Trends Genet* **2004**, *20* (1), 33−43.
(17) Chen, Y.; Guo, H.; Terajima, M.; Banerjee, P.; Liu, X.; Yu, J.; Momin, A. A.; Katayama, H.; Hanash, S. M.; Burns, A. R.; Fields, G. B.; Yamauchi, M.; Kurie, J. M. Lysyl Hydroxylase 2 Is Secreted by Tumor Cells and Can Modify Collagen in the Extracellular Space. *J. Biol. Chem.* **2016**, *291* (50), 25799−25808.
(18) Pankova, D.; Chen, Y.; Terajima, M.; Schliekelman, M. J.; Baird, B. N.; Fahrenholtz, M.; Sun, L.; Gill, B. J.; Vadakkan, T. J.; Kim, M. P.; Ahn, Y. H.; Roybal, J. D.; Liu, X.; Parra Cuentas, E. R.; Rodriguez, J.; Wistuba, I. I.; Creighton, C. J.; Gibbons, D. L.; Hicks, J. M.; Dickinson, M. E.; West, J. L.; Grande-Allen, K. J.; Hanash, S. M.; Yamauchi, M.; Kurie, J. M. Cancer-Associated Fibroblasts Induce a Collagen Cross-link Switch in Tumor Stroma. *Mol. Cancer Res.* **2016**, *14* (3), 287−95.
(19) Zuurmond, A.-M; van der Slot-Verhoeven, A. J.; van Dura, E. A.; De Groot, J.; Bank, R. A. Minoxidil exerts different inhibitory effects on gene expression of lysyl hydroxylase 1, 2, and 3: implications for collagen cross-linking and treatment of fibrosis. *Matrix Biol.* **2005**, *24*, 261−270.
(20) Pfeffer, T.; Lignelli, E.; Inoue, H.; Mizikova, I.; Surate Solaligue, D. E.; Steenbock, H.; Myti, D.; Vadasz, I.; Herold, S.; Seeger, W.; Brinckmann, J.; Morty, R. E. Minoxidil Cannot Be Used To Target Lysyl Hydroxylases during Postnatal Mouse Lung Development: A Cautionary Note. *J. Pharmacol Exp Ther.* **2020**, *375*, 478−487.
(21) Du, Y.; Khan, M.; Fang, N.; Ma, F.; Du, H.; Tan, Z.; Wang, H.; Yin, S.; Wei, X. Berberine Attenuates Cell Motility via Inhibiting Inflammation-Mediated Lysyl Hydroxylase-2 and Glycolysis. *Front. Pharmacol.* **2022**, *13*, 856777.
(22) Thaler, R.; Spitzer, S.; Rumpler, M.; Fratzl-Zelman, N.; Klaushofer, K.; Paschalis, E. P.; Varga, F. Differential effects of homocysteine and beta aminopropionitrile on preosteoblastic MC3T3-E1 cells. *Bone* **2010**, *46*, 703−709.
(23) Bennett, I.; Broom, N. J. P.; Cassels, R.; Elder, J. S.; Masson, N. D.; O'Hanlon, P. J. Synthesis and antibacterial properties of b-diketone acrylate bioisosteres of pseudomonic acid A. *Bioorg. Med. Chem. Lett.* **1999**, *9*, 1847−1852.
(24) Sheikh, J.; Parvez, A.; Juneja, H.; Ingle, V.; Chohan, Z.; Youssoufi, M.; Ben Hadda, T. Synthesis, biopharmaceutical characterization, antimicrobial and antioxidant activities of 1-(40-O-b-D-glucopyranosyloxy-20 -hydroxyphenyl)-3-aryl-propane-1,3-diones. *Eur. J. Med. Chem.* **2011**, *46*, 1390−1399.
(25) Diana, G. D.; Carabateas, P. M.; Johnson, R. E.; Williams, G. L.; Pancic, F.; Collins, J. C. Antiviral activity of some b-diketones. 4. Benzyldiketones. In vitro activity against both RNA and DNA viruses. *J. Med. Chem.* **1978**, *21*, 889−894.
(26) Crouse, G. D.; McGowan, M. J.; Boisvenue, R. J. Polyflouro 1,3- diketones as systemic insecticides. *J. Med. Chem.* **1989**, *32*, 2148−2151.
(27) Nishiyama, T.; Shiotsu, S.; Tsujita, H. Antioxidative activity and active site of 1,3-indanediones with the b-diketone moiety. *Polym. Degrad. Stab.* **2002**, *76*, 435−439.
(28) Pivarcsik, T.; Toth, G.; Szemeredi, N.; Bogdanov, A.; Spengler, G.; Kljun, J.; Kladnik, J.; Turel, I.; Enyedy, E. A. Comparison of Solution Chemical Properties and Biological Activity of Ruthenium Complexes of Selected β-Diketone, 8-Hydroxyquinoline and Pyrithione Ligands. *Pharmaceuticals* **2021**, *14*, 518.
(29) Kel'in, A. V. Recent Advances in the Synthesis of 1,3-Diketones. *Curr. Org. Chem.* **2003**, *7*, 1691−1711.
(30) Lim, D.; Fang, F.; Zhou, G.; Coltart, D. M. Direct carbon-carbon bond formation via soft enolization: a facile and efficient synthesis of 1,3-diketones. *Org. Lett.* **2007**, *9* (21), 4139−42.
(31) Devkota, A. K.; Veloria, J. R.; Guo, H. F.; Kurie, J. M.; Cho, E. J.; Dalby, K. N. Development of a High-Throughput Lysyl Hydroxylase (LH) Assay and Identification of Small-Molecule Inhibitors against LH2. *SLAS Discov* **2019**, *24* (4), 484−491.
(32) Maghsoud, Y.; Vázquez-Montelongo, E. A.; Yang, X.; Liu, C.; Jing, Z.; Lee, J.; Harger, M.; Smith, A. K.; Espinoza, M.; Guo, H.-F.; Kurie, J. M.; Dalby, K. N.; Ren, P.; Cisneros, G. A. Computational Investigation of a Series of Small Molecules as Potential Compounds for Lysyl hydroxylase-2 (LH2) Inhibition. *J. Chem. Inf. Model.* **2023**, *63* (3), 986−1001.
(33) Savastano, M.; García-Gallarín, C.; Giorgi, C.; Gratteri, P.; López de la Torre, M. D.; Bazzicalupi, C.; Bianchi, A.; Melguizo, M. Solid State and Solution Study on the Formation of Inorganic Anion Complexes with a Series of Tetrazine-Based Ligands. *Molecules* **2019**, *24*, 2247.
(34) Parkin, A.; Oswald, I. D. H.; Parsons, S. Structures of piperazine, piperidine and morpholine. *Acta Crystallogr.* **2004**, *B60*, 219−227.
(35) Lan, N.; Lu, Y.; Zhang, Y.; Pu, S.; Xi, H.; Nie, X.; Liu, J.; Yuan, W. FTO - A Common Genetic Basis for Obesity and Cancer. *Front Genet* **2020**, *11*, 559138.
(36) Couture, J. F.; Collazo, E.; Ortiz-Tello, P. A.; Brunzelle, J. S.; Trievel, R. C. Specificity and mechanism of JMJD2A, a trimethyllysine-specific histone demethylase. *Nat. Struct Mol. Biol.* **2007**, *14* (8), 689−95.
(37) Fong, G. H.; Takeda, K. Role and regulation of prolyl hydroxylase domain proteins. *Cell Death Differ.* **2008**, *15* (4), 635−41.
(38) Luther, K. B.; Hulsmeier, A. J.; Schegg, B.; Deuber, S. A.; Raoult, D.; Hennet, T. Mimivirus collagen is modified by bifunctional lysyl hydroxylase and glycosyltransferase enzyme. *J. Biol. Chem.* **2011**, *286* (51), 43701−43709.
(39) Liu, W.; Zhang, T.; Guo, L.; Wang, Y.; Yang, Y. Lysyl hydroxylases are transcription targets for GATA3 driving lung cancer cell metastasis. *Sci. Rep* **2018**, *8*, 11905.
(40) Wang, Z.; Fan, G.; Zhu, H.; Yu, L.; She, D.; Wei, Y.; Huang, J.; Li, T.; Zhan, S.; Zhou, S.; Zhu, Y.; Wang, Y.; Chen, X.; Zhao, J.; Zhou, G. PLOD2 high expression associates with immune infiltration and facilitates cancer progression in osteosarcoma. *Front. Oncol.* **2022**, *12*, 980390.
(41) Gibbons, D. L.; Lin, W.; Creighton, C. J.; Rizvi, Z. H.; Gregory, P. A.; Goodall, G. J.; Thilaganathan, N.; Du, L.; Zhang, Y.; Pertsemlidis, A.; Kurie, J. M. Contextual extracellular cues promote tumor cell EMT and metastasis by regulating miR-200 family expression. *Genes Dev.* **2009**, *23*, 2140−2151.

https://doi.org/10.1021/acsmedchemlett.3c00305
ACS Med. Chem. Lett. 2023, 14, 1396−1403